MONTHLY NOTICES of the Royal Astronomical Society

Magnetic field structure in simulations of ram pressure stripped galaxies

Journal:	*Monthly Notices of the Royal Astronomical Society*
Manuscript ID	MN-19-4489-MJ
Manuscript type:	Main Journal
Date Submitted by the Author:	10-Dec-2019
Complete List of Authors:	Ramos-Martínez, Mariana; Instituto de Radioastronomia y Astrofisica - UNAM, Gómez, Gilberto; Centro de Radioastronomía y Astrofisica, UNAM,
Keywords:	(magnetohydrodynamics) MHD < Physical Data and Processes, galaxies: evolution < Galaxies, galaxies: magnetic fields < Galaxies, galaxies: ISM < Galaxies, galaxies: interactions < Galaxies

MNRAS 000, 1–15 (2019) Preprint 10 December 2019 Compiled using MNRAS LATEX style file v3.0

Magnetic field structure in simulations of ram pressure stripped galaxies

Mariana Ramos-Martínez,[1⋆] Gilberto C. Gómez,[1]
[1] Instituto de Radioastronomía y Astrofísica, Universidad Nacional Autónoma de México, Apdo. Postal 3-72, Morelia Mich. 58089, México

Accepted XXX. Received YYY; in original form ZZZ

ABSTRACT

We performed 3D magnetohydrodynamic (MHD) simulations of disc galaxies subject to ram pressure stripping (RPS), with different disc inclinations to study the evolution of the magnetic field (MF) and its impact on the gas stripping. When the intracluster medium (ICM) wind hits a galaxy, the gas in the disc is compressed, leading to an enhancement of the MF intensity in the disc. In models with low disc inclinations the gas is swept in ring-like structures that are distorted by the wind producing a filamentary and broad tail, dragging the MF with it. Models with high disc inclinations develope narrower tails instead, where the MF lines emerge outside of the galactic plane and wrap around the disc in the downstream side. Also, the field lines are compressed in the interaction zone and on the opposite side are stretched when pushed by the wind. A model with an intermediate inclination presents an evolution that is a combination of the cases with low and high inclinations: magnetized gas is removed in rings first, the gas tail develops filaments although it becomes narrower like the high inclined models. The ICM is magnetized from 0.2 to $0.7\mu G$, where low inclined discs contribute the most. We also obtained maps of the synchrotron emission and polarization vectors. The synchrotron emission presents an asymmetric distribution that is truncated in the disc, similar to some Virgo galaxies, while the polarization vectors trace very accurately the MF distribution of the simulations.

Key words: MHD – galaxies: evolution – galaxies: magnetic fields – galaxies: ISM – galaxies: interactions

1 INTRODUCTION

Magnetic fields (MFs) have been observed in galaxies from polarized emission in optical (Scarrott et al. 1987; Fendt et al. 1998; Fosalba et al. 2002), infrared (Jones 2000), submillimeter (Greaves et al. 2000), and radio wavelengths (Vollmer et al. 2004, 2010, 2013). In optical wavelengths, the starlight is polarized by elongated dust grains with their major axis aligned with the magnetic field lines perpendicular to the line-of-sight (LOS), while the dust grains emit their own linearly polarized waves at far infrared and submillimeter, without contributions by polarized scattered light (Vallée 1997). Combining information obtained with different techniques like Faraday rotation, Zeeman effect, and polarized radio synchrotron emission, it is possible to develop a model for the 3D structure of MFs in galactic discs. It is known that MFs in spirals have an ordered component, i.e. with a constant and coherent direction within the telescope beam (large-scale), and a random or turbulent component that has been amplified and tangled by turbulent gas flows changing its direction within the telescope beam (small-scale) and its orientation can be isotropic or anisotropic (Beck 2005a, Beck & Wielebinski 2013 and references therein). The anisotropic turbulent field can be originated from an isotropic field that has been affected by compression or shearing of gas. In spirals, the average total field strength is $\sim 9\,\mu G$ (Niklas 1995) and the regular field strength is $1-5\,\mu G$ (Beck & Wielebinski 2013). In radio-faint galaxies like M31 and M33 the total field is $6\,\mu G$ (Gießübel 2012; Tabatabaei et al. 2008), in gas rich spiral galaxies the total field is $20-30\,\mu G$ (Fletcher et al. 2011; Frick et al. 2016), for bright galaxies $\sim 17\,\mu G$ (Fletcher 2010), in blue compact dwarf galaxies $10-20\,\mu G$ (Klein et al. 1991), and the strongest total fields are found in starburst and barred galaxies with $50-100\,\mu G$ (Adebahr et al. 2013; Chyży & Beck 2004; Beck et al. 2005). In our Galaxy, the regular field is $\sim 2\,\mu G$ (Han et al. 2006; Orlando & Strong 2013) and the random component has a mean strength of $4-6\,\mu G$ (Rand & Kulkarni 1989; Ohno & Shibata 1993; Han et al. 2004).

⋆ E-mail: m.ramos@irya.unam.mx (MRM)

The MFs in other galaxies have been mainly studied in radio frequencies through synchrotron emission. This radio emission is produced when relativistic particles (electrons or cosmic rays, CR) with density $n_{\rm cr}$ gyrate around the MF lines: $\varepsilon \propto n_{\rm cr} B_{\perp}^{(p+1)/2}$, where $B_{\perp}$ is the MF component perpendicular to the LOS, p is the spectral index of the distribution of cosmic ray electrons, and ε is the emissivity of the synchrotron emission. The linearly polarized synchrotron emission is generated from the regular component of the MF. In observations of spiral galaxies the degree of polarization on average is low in the spiral arms, so the random field is assumed to be stronger there, up to five times the intensity of the ordered field, whilst in the interarm region the degree of polarization is higher, hence the ordered field should dominate. Additionally, it has been observed that the ordered MF shows a spiral pattern that is offset from the spiral arms of gas and stars (Beck 2005a). Given that the regular field has a large-scale, interactions with the environment would have an impact in the polarized synchrotron emission.

Since the MF is frozen into the gas, any interaction in the ISM would be reflected on the MF. For example, during ram pressure stripping, the gas of the galaxy is compressed before it is swept, and hence the MF is also compressed and its intensity enhanced (Otmianowska-Mazur & Vollmer 2003). Studies of the synchrotron and polarization emission of spirals have been performed in the Virgo Cluster (Vollmer et al. 2010 and Vollmer et al. 2013), since it is the rich cluster closest to our Galaxy and it contains undisturbed and interacting galaxies, some of which are good candidates to be under the effect of RPS. As is shown in Vollmer et al. (2010), the radio continuum emission has a sharp distribution where the edges coincide with HI distribution, such that the synchrotron traces the interaction of a galaxy with its environment, like RPS and interacting galaxies seen edge-on present a radio continuum emission that extends a little farther than the HI.

From deep VLA observations at 4.86 GHz, Vollmer et al. 2004, 2007 and Chyży et al. 2006, 2007 showed that the distribution of polarized radio continuum emission of 8 Virgo cluster spiral galaxies is strongly asymmetric, with elongated ridges located in the outer galactic disc, which is different for field galaxies where the distribution is generally relatively symmetric and strongest in the interarm regions (Beck 2005b).

Murphy et al. (2009) investigated the radio/FIR relation in galaxies of the Virgo Cluster, possibly affected or with signs of RPS. Galaxies interacting with the ICM show a radio emission deficit on the leading side of the ISM-ICM interaction due to ram pressure. Also, galaxies from the Virgo Cluster exhibit highly polarized radio emission on the upstream side of the ISM-ICM interaction, e.g. NGC 4522 (Chyży et al. 2007; Vollmer et al. 2007). Some Virgo galaxies (NGC 4254, NGC 4388, and NGC 4402) present highly polarized regions that coincide with local radio continuum enhancements and interior to the radio-deficit regions. In the sample of Murphy et al. (2009), it is seen that while the local radio deficit increases, the global radio flux density is enhanced by a factor of $2 - 3$ compared to isolated galaxies, which could be related to magnetic field compression and CRs that are swept and reaccelerated by the ICM-wind generating synchrotron tails. Also in Vollmer et al. (2013), it was found that even when active ram pressure stripping has no influence on the spectral index, it enhances the global radio continuum emission with respect to the FIR emission by up to a factor of 2, while an accreting gas envelope may or may not enhance the radio continuum emission with respect to the FIR emission.

MFs are present in the ICM and their strength has been observationally measured and constrained to be of the order of μG (reviewed in Carilli & Taylor 2002; Govoni & Feretti 2004; Kronberg 2005; Ryu et al. 2012). Indirect evidence for the presence of cluster MFs and their strengths comes from cluster radio halos produced by the synchrotron radiation (Miley 1980; Giovannini et al. 1993; Feretti et al. 1999; Govoni & Feretti 2004). The integrated cluster MF can be directly measured using the Faraday rotation measure (RM). Faraday RM shows that ICM magnetic fields are of $\sim \mu G$ strengths coherent over scales of tens of kpc (Vallée et al. 1986, 1987; Kim et al. 1990, 1991; Taylor & Perley 1993; Taylor et al. 1994, 2001; Clarke et al. 2001; Rudnick & Blundell 2003; Murgia et al. 2004; Govoni et al. 2010; Bonafede et al. 2010, 2011, 2013; Vacca et al. 2012) In a phenomenon such as RPS, it is expected that the MFs are dragged with the stripped gas and hence the tails can magnetize or maintain the magnetic fields in the ICM.

On the theoretical side, Ruszkowski et al. (2014) presented simulations of RPS with a magnetized ICM and found that the MF can affect the morphology of the stripped gas tail, since they observed narrower tails than in purely hydrodynamic (HD) simulations. Pfrommer & Jonathan Dursi (2010) also showed magnetohydrodynamics (MHD) simulations in which the galaxies are moving in a magnetized ICM. The galaxies in their simulations swept the field lines where polarized radiation is generated. This is used to map the orientation of the MF in clusters. In these cases, the MF has been implemented only in the ICM and not in the discs. Some examples of models with magnetized discs are from Vollmer et al. (2006, 2007) and Soida et al. (2006), which used the method of Otmianowska-Mazur & Vollmer (2003) where a toroidal galactic MF is evolved via the induction equation using a grid code with the velocity field of the particles, so that the MF is advected with the gas. Even if the effect of the MF over the gas dynamics has not been taken into account, this method has been useful to explain the polarized radiation in radio that is observed in some galaxies that may be affected by the RPS, as in the case of NGC 4522 (Vollmer et al. 2006). Additionally, Tonnesen & Stone (2014) performed MHD simulations for the RPS including galactic MF, but the ICM was not magnetized. They found that MFs do not alter or dramatically change the stripping rate of the gas disc compared to pure HD simulations. Nevertheless, the MFs have an impact in the mixing of gas throughout the tail. Since it inhibits the mixing of the gas tail with the ICM, the unmixed gas survives at large distances from the disc. Additionally, the RPS may help magnetize the ICM up to a few μG. Vijayaraghavan & Sarazin (2017) presented MHD simulations where both ICM and ISM are magnetized with different MF orientations and with/without thermal conduction. From their models, the MF orientation changes the morphology of the gas tails: for an MF parallel to the wind motion, the stripped tails are long and narrow compared to case where the MF lines are perpendicular to the ICM motion. Also, the MFs act as a shield in the stripped tails preventing their rapid evaporation in the ICM. Including or not thermal conduction in their simulations represents a difference of $10-20\%$ in the gas loss rate, which means that the dominant process in removing the gas from the galaxy is the RPS. In Ramos-Martínez et al. (2018), we presented 3D MHD simulations of RPS with galactic MFs only, where the main effect of including a galactic MF is a flared disc which yields to the emergence of oblique shocks when the ICM hits the disc, leading to the funnelling of gas towards the central regions of the galaxy before is stripped. Additionally, the MFs modify the shape and structure of the gas tail, showing a smooth appearance whilst in a pure-hydro run, the tail looks clumpier.

In this manuscript we analysed the structure of the stripped tails when varying the inclination of disc galaxies interacting with the ICM. The evolution of the galactic MF is studied in the scheme of RPS and how much is the ICM magnetized depending on the inclination of a galaxy. Synchrotron emission maps are generated from the models as well as the infered magnetic field B-vectors.

2 MODEL

In the present study, five models were carried out to represent the RPS of disc galaxies with different inclination angles with respect to the relative motion of the galaxy with respect to the ICM: 0, 20, 45, 70 and 90^{o}. The models were performed in 3D with 9 levels of refinement, in a box of size 120 kpc in each direction so that the effective resolution in the simulation is 0.23 kpc. Each galaxy is at rest and the ICM flows as a wind to simulate the galaxy falling towards a cluster.

2.1 Initial Conditions

To set up the initial conditions of the models, the procedure from Ramos-Martínez et al. (2018) was used for an M33-like galaxy with a rotation curve of $\sim 110-120\,\mathrm{km\ s^{-1}}$ subjected to RPS. The galaxy consists of a gas disc that is initially set up in rotational equilibrium with the gravitational force, magnetic tension, centrifugal force and pressure gradient:

$$\frac{v_\phi^2(r,z)}{r} = \frac{\partial\Phi}{\partial r} + \frac{1}{\rho(r,z)}\left[\frac{\partial P}{\partial r} + \frac{2P_B(r,z)}{r}\right], \qquad (1)$$

where the total pressure P is the sum of the thermal ($P_{th} = c_s^2\rho(r,z)$, with $c_s \approx 8\,\mathrm{km\ s^{-1}}$ the constant sound speed) and magnetic (P_B) pressures. The magnetic pressure is given by

$$P_{B,inner} = P_{B0}\left[1 - \mathrm{erf}\left(\frac{R}{r_b}\right)\right] \quad \text{for } R < r_b\text{, and} \qquad (2)$$

$$P_{B,outer} = \frac{P_{B0}\, n}{(n+n_c)}, \qquad (3)$$

where $R = \sqrt{r^2+z^2}$, $r_b = b_1/3$, $b_1 = 0.85\,\mathrm{kpc}$ (see table 1 from Ramos-Martínez et al. 2018), $P_{B0} = 1.75 \times 10^{-13}\,\mathrm{dyn\,cm^{-2}}$, $n = \rho/(\mu m_{\mathrm{H}})$ and $n_c = 0.04\,\mathrm{cm^{-3}}$. The density and velocity profile are defined first in the galactic midplane and then the distribution at $z \neq 0$ is obtained assuming magnetohydrostatic equilibrium and an isothermal equation of state,

$$\frac{\partial P}{\partial z} = -\rho\frac{\partial\Phi}{\partial z}. \qquad (4)$$

The rotation velocity at any z is given by (Gómez & Cox 2002):

$$v_\phi^2(r,z) = v_\phi^2(r,0) - v_A^2(r,0) + v_A^2(r,z), \qquad (5)$$

where v_A is the Álfven velocity ($v_A = \sqrt{2P_B/\rho}$).

The galactic magnetic field (MF) is initially divided in two regimes: a random component for the central part of the galaxy and a regular field in the disc. The random MF for $r < b_1$ has a distribution $\mathbf{B_{inner}} = \nabla\times\mathbf{A}$, where $\mathbf{A}$ is the vector potential with random magnitude and orientation. For the rest of the disc, the field has a toroidal configuration where its strength depends on the gas density according to eq. 3. The MF strength for the initial conditions is $B \sim 1\,\mu G$ at $r < 10\,\mathrm{kpc}$, which is in the lower limit of the ordered field for spiral galaxies, and $B \lesssim 0.5\,\mu G$ between $10\,\mathrm{kpc} < r < 20\,\mathrm{kpc}$ (fig. 1). Although the random component of the MF in spiral galaxies has an important contribution to the total MF intensity, the length scale of the fluctuations in the random field is small, e.g. $10-100\,\mathrm{pc}$ for the Milky Way (Ohno & Shibata 1993), so the resolution achieved in these simulations was not enough to model this component for the rest of the disc.

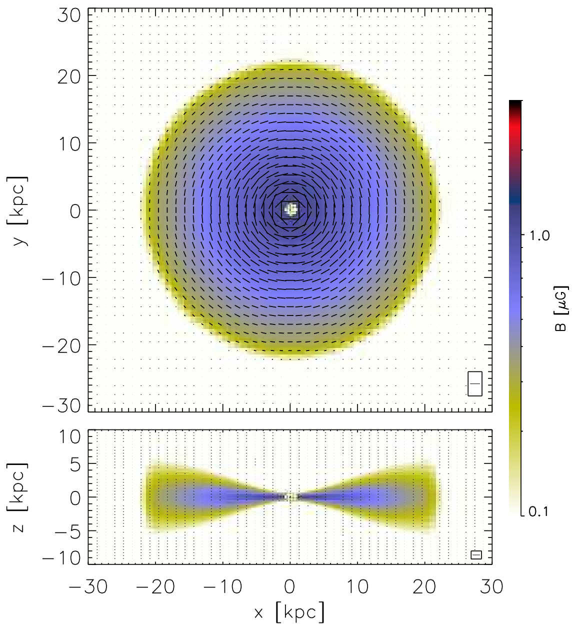

Figure 1. Magnetic field strength at the initial condition for all models in a $z=0$ (*top*) and $y=0$ (*bottom*) cut. The box in the bottom of the panels shows an MF line with a strength of $0.5\,\mu G$.

2.2 ICM conditions

The ICM is modeled as a wind while the disc is at rest, simulating the falling of the galaxy towards a cluster center. The ICM-wind has a constant density with $n_{\rm ICM} = 10^{-5}\,{\rm cm}^{-3}$ and a velocity profile that increases linearly in time from $300\,{\rm km\ s}^{-1}$ at $t = 0$ to $1000\,{\rm km\ s}^{-1}$ in 700 Myr and moves in the $+z$-direction. We present five models with different galaxy inclinations with respect to the wind direction. The model A0 represents a galaxy with its disc plane parallel to the $z = 0$ plane, i.e. an inclination of $0^{\rm o}$ or a face-on interaction with the wind. Models A20, A45 and A70 are discs with inclinations of 20, 45 and $70^{\rm o}$, respectively, and finally A90 is a disc with an inclination of $90^{\rm o}$ with respect to the $z = 0$ plane, which is a completely edge-on interaction with the wind.

3 EVOLUTION OF THE MAGNETIC FIELD

When the ICM-wind is switched-on and hits the galactic disc, the compression exerted by the wind enhances the MF strength in all the models by a factor of ~ 3 in the shock front. Depending on the geometry of the model, the shocked layer of gas can be present at all radii, as in simulation A0 where the compression is visible in $z < 0$ (left fig. 2), or partially in the disc, as in models A20 and A45 at the region between $z < 0$ and $x < 0$ (left figs. 3 and 4). This is more clearly seen in models A70 and A90 at $z \sim -20\,{\rm kpc}$ (left figs. 5 and 6).

Since the wind accelerates as it flows, it starts to remove the material from the outskirts ($20\,{\rm kpc} > r > 10\,{\rm kpc}$) where a tail of gas appears in the downstream side. At 500 Myr, in the simulations A0 and A20, where the interaction with the wind is (nearly) face-on, and in model A45 (medium inclination) the gas is swept from the galaxy up to a height of $\sim 20\,{\rm kpc}$ from the galactic midplane in ring-like structures parallel to the disc plane and also the general distribution of the gas has a cap shape as seen in the xz-plane (middle panels in figs. 2, 3, and 4). Also, the magnetic field is dragged with the gas, which helps magnetize the downstream side of the tail up to $z \sim 20\,{\rm kpc}$ with a strength of $B \approx 0.4 - 0.7\,\mu G$, as can be seen in the bottom middle panels of figs. 2, 3, 4. At $z \gtrsim 10\,{\rm kpc}$ the rings start to show some slight perturbations along the direction of the wind, away from the disc where the stripped gas is less influenced by the potential well of the galaxy. The disc of the galaxies show an enhancement of the field from $B(t = 0) \approx 0.8 - 1\,\mu G$ to $B(t \sim 500\,{\rm Myr}) \approx 2.5\,\mu G$ in $r \lesssim 10\,{\rm kpc}$, that is, a factor of $\sim 2 - 3$. On the other hand, models A70 and A90 do not present a very extended tail at $t \geq 500\,{\rm Myr}$, as can be observed in an edge-on view of the galaxies on the xz-plane (middle panels in figs. 5 and 6). Instead, the gas disc shows asymmetries compared to the initial density distribution, spreading out to $z \sim 20 - 40\,{\rm kpc}$ but with a low surface densities ($\Sigma < 10^{-4.5}\,{\rm g\,cm}^{-2}$). Additionally, in models A70 and A90, the MF intensity increases a factor of $\sim 2 - 3$ ($B \approx 1.5 - 3\,\mu G$) in the upstream side of the interaction ($-10\,{\rm kpc} < z < 0$) while in downstream side ($z = 0 - 20\,{\rm kpc}$) the strength of the field does not change significantly, at $B \approx 0.8 - 1\,\mu G$ (bottom middle panels in figs. 5 and 6).

At $t = 890\,{\rm Myr}$, the wind reaches velocities of $\sim 1000\,{\rm km\ s}^{-1}$ in $z = 0$ and, for models A0, A20 and A45, it moves the rings of gas above and farther away of the galaxy, showing tails of at least 60 kpc in length (right panels in figs. 2, 3 and 4). Due to the interaction with the accelerated wind, the rings are distorted in the vertical (z) direction giving a filamentary structure to the tail and, since these filaments are the densest structures ($\Sigma \sim 10^{-3.6}\,{\rm g\,cm}^{-2}$), here the MF has values ranging from $B \approx 0.3 - 0.4\,\mu G$ to $0.7\,\mu G$ (figs 2, 3 and 4, bottom right panels). At intermediate heights in the tails of models A0 and A20 ($z = 15 - 30\,{\rm kpc}$), the field strength drops to $B \lesssim 0.2\,\mu G$ since less gas is swept from the disc and the surface density also decreases. Simulations A70 and A90 at $t = 890\,{\rm Myr}$ did not develop very prominent or extended tails, where the displaced gas of the disc lies between $z = 20 - 60\,{\rm kpc}$ on figs. 5 and 6 (right panels). Also the tail is poorly magnetized with $B \lesssim 0.2 - 0.3\,\mu G$ compared to the (nearly) face-on models A0 and A20. Model A45 shows a behaviour that is a combination of both low and high tilted discs: this model shows filaments of gas similar to the ones observed in models A0 and A20 and is more extended on the trailing side of the wind-disc interaction ($x > 0$) as in model A70. Also in A45, the MF in the tail has low values ($B \sim 0.3\,\mu G$) although the magnetization is more homogeneous at $z > 20\,{\rm kpc}$. The tail in model A45 is narrower than in simulations A0 and A20 but a bit broader than in A70 and A90, i.e. the width of the tails in these simulations decreases with increasing the initial inclination of the disc.

Observing the surface of the disc for all the models, that is in the xy-plane for models A0, A20 and A45 (fig. 7) and the yz-plane for A70 and A90 (fig. 8) and again for A45, the gas in the remnant disc with $\Sigma > 10^{-3.5}\,{\rm g\,cm}^{-2}$ in models A70 and A90 show more structure than in the tails, for example spiral-like features, contrary to A0 and A20 which show discs with a smoother gas distribution. The model A45 exhibits a weaker spiral structure in the disc compared to A70 and A90 (figs. 7 and 8). These type of spirals observed mainly in simulations A70 and A90 could be related to the fact that in these (nearly) edge-on interactions the ram pressure has to compete against the circular velocity of the discs: if the wind reaches the portion of the disc where the gas sense of rotation has the same direction as the ram pressure, then the gas is stripped slightly easier and displaced farther of the galaxy; while in the side of the disc whose rotation opposes to the motion of the wind, the rotation itself prevents the gas of being swept and instead more material accumulates in that part of the galaxy, generating a shape similar to spiral arms (although our simulation does not have self gravity).

In all the models, a remnant gaseous disc of size $r \lesssim 10\,{\rm kpc}$ is observed at the end of the simulation. The (nearly) face-on cases (A0 and A20) present an enhanced MF strength of $B \sim 2 - 3\,\mu G$ close to the galactic midplane, while in A70 and A90 the MF is $B \sim 3\,\mu G$ on the leading side of the shock, specially in the spiral structure, and $B \sim 1 - 1.5\,\mu G$ throughout most of the disc, also for model A45 the MF reaches its highest values in the disc spirals, similarly to the (nearly) edge on cases. The enhancement of the MF strength is a factor of ~ 3 compared to the initial condition. Observations of late-type spiral galaxies in clusters showed that they have a radio continuum emission enhanced by a factor up to ~ 5 compared to isolated spirals (Gavazzi & Jaffe 1986; Gavazzi & Boselli 1999) and this could be either by an increase in the star formation activity,

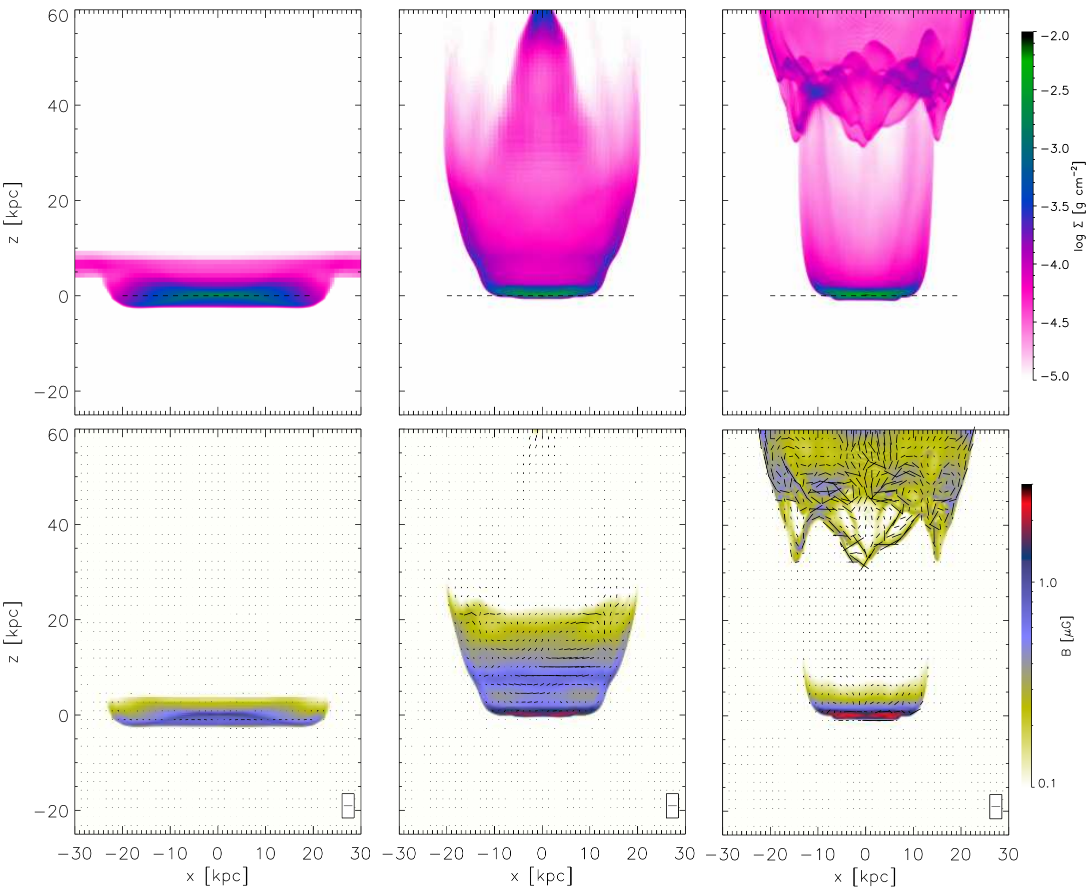

Figure 2. Gas surface density (*top row*) and magnetic field strength and direction (*bottom row*) for disc A0 at $t = 110$ Myr (*left column*), $t = 570$ Myr (*centre column*) and $t = 890$ Myr (*right column*) in the xz-plane. The dashed lines in the top panels represents the initial size of the disc: $r = 20$ kpc. The box in the bottom panels shows an MF line with a strength of $0.5\,\mu G$.

producing more cosmic rays from supernovae, an enhancement of the MF, or a combination of both.

To better determine in which model the ICM is magnetized the most, we calculate the magnetic energy in the tails. The magnetic energy is obtained from the gas located above a height of $h > 5$ kpc from the galactic midplane in all models (except A90), however, given that the tails have different extensions and shapes depending on the initial disc inclination, for models A0/A20/A45 it was considered the gas within a radius of $r < 25$ kpc, for model A70 the gas at $|x| < 15$ kpc and $|y| < 25$ kpc and finally for model A90 $|x| < 10$ kpc, $|y| < 20$ kpc and $z > 20$ kpc given that this model exhibits the narrowest tail. Fig. 9 shows the magnetic energy $E_{\rm mag}$ as function of the volumetric density n for the swept gas. In the case of low inclination discs (A0 and A20, top panels in fig. 9), the magnetic energy is spread through a wide range of values between 10^{47} to 10^{49} erg, reaching close to 10^{50} erg in some cases. Also, since the gas of these models is stripped in ring-like features that evolve into a filamentary structure, the tails present regions of high and low density, hence we have a high number of cells extending over a range in densities of 10^{-4} to $\gtrsim 10^{-2}\,{\rm cm}^{-3}$ and with higher magnetic energy compared to models A70 and A90 (bottom panels in fig. 9). For A70 and A90, we have less cells with magnetic energy $E_{\rm mag} \sim 10^{47} - 10^{48}$ erg outside of the discs (also with low densities 10^{-4} to $10^{-3}\,{\rm cm}^{-3}$). However, the higher increase of magnetic energy in these models lies in the discs (not shown in the graphics of fig. 9) since the MF, compressed with the disc in the upstream side of the interaction, increases a factor of ~ 1.2 compared to models A0 and A20. From this simulations it is observed that (nearly) face-on disc-wind interaction tend to magnetize more the ambient than (nearly) edge-on models.

3.1 Magnetic field lines

As mentioned above, in the (nearly) face-on models the gas is removed in ring-like structures dragging the MF with it. As time goes by and the wind accelerates, the rings are perturbed by the wind and filaments appear along the gas tail. In figs. 2 and 3 (bottom right in both images) it can be observed, on an xz view, that the MF lines are aligned with the filaments, similarly to the results obtained by Ruszkowski et al. (2014). On a view over the xy-plane from figs. 7 (bottom panels), the MF lines still keep their initial circular configuration, such that these are distorted in the z-axis, parallel to the wind motion. However, the model A20 shows some asymmetries for the distribution of the MF

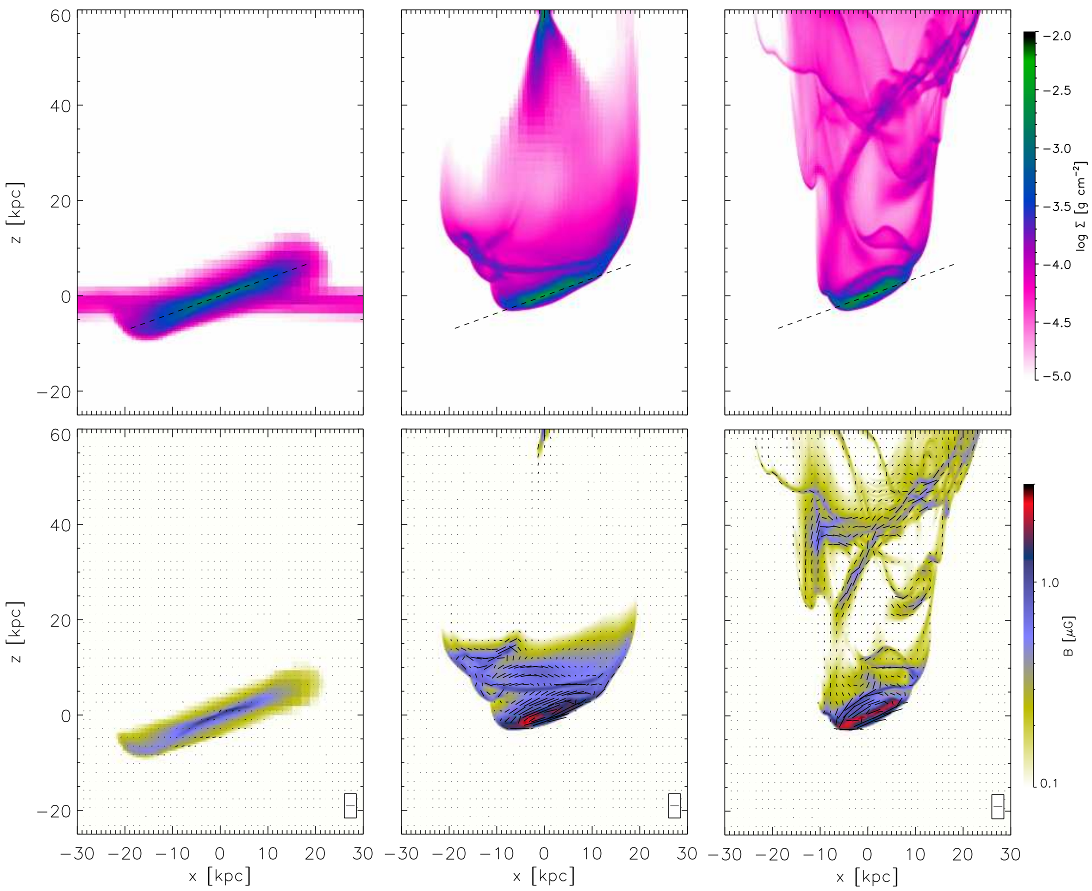

Figure 3. Same as fig. 2 for the A20 simulation.

lines (lower right panel in fig. 7) that are probably due to projection effects or the inclination of the disc.

In the case of the (nearly) edge-on models (A70 and A90), when the discs are seen in the xz-plane (lower panels in figs. 5 and 6), the MF lines resemble a water fountain: they have a concave shape in the upstream side and wrap around the disc at higher $|z|$ since the wind flows parallel or nearly to the plane of the disc and sweeps the gas above and below the galaxy midplane more easily than gas closer to the galactic plane. Observing these models on the yz-plane in figs. 8 (bottom panels), the MF is compressed in the upstream side and more extended by the wind in the downstream side giving an ellipsoid morphology to the MF lines. Similarly to model A20, this effect is more evident in model A70 due to the inclination of the disc.

The model A45, as it has been mentioned, is a combination of both low and high inclined discs, that is, when observing the distribution of the MF lines over the xy (fig. 7) and yz (fig. 8) planes, the MF presents a circular configuration like models A0 and A20 although they are slightly compressed on the leading side of the shock and extended in the opposite direction as in A70 and A90.

4 SYNTHETIC SYNCHROTRON EMISSION AND POLARIZATION

The total synchrotron emission of the models is obtained by integrating the emissivity:

$$\varepsilon \propto n_{\rm cr} B_{\perp}^{(p+1)/2}\,, \qquad (6)$$

where $n_{\rm cr}$ is the cosmic ray electrons (CR) density distribution, $B_{\perp}$ is the MF component perpendicular to the line of sight (LOS), and $p = 2.5$ is the assumed spectral index of the distribution of cosmic ray electrons. Here, $n_{\rm cr}$ is assumed constant since it is expected that the less energetic CRs, with a gyroradius smaller than the size of the galaxy, are dragged with the MF when the wind is sweeping the material (additionally, the distribution of the CRs at high z is uncertain; Ferrière 1998).

Fig. 10 shows the synchrotron emission over the gas surface density for all the models at $t = 570\,$Myr. The distribution of the synchrotron emission is asymmetric. On the side of the galaxy that is facing the ICM wind, the emission is compressed with sharp edges while in the opposite side it is extended developing a synchrotron tail. However, the distribution in models A0 and A20 (top panels in fig. 10) presents larger and broader tails than in A70 and A90 (bottom panels in fig. 10). The synchrotron tails of models A45 and A70 have a similar morphology, i.e. is larger on the

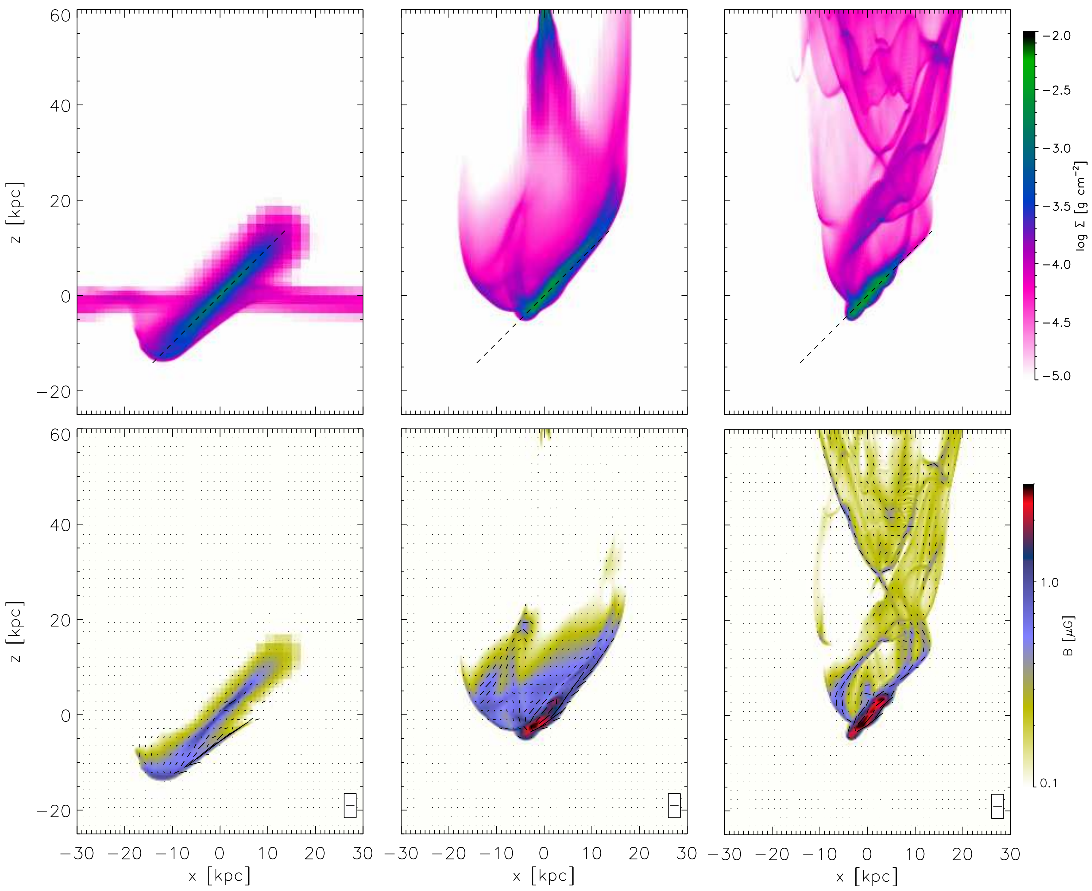

Figure 4. Same as fig. 2 for the A45 simulation.

left side ($x < 0$ in fig. 10) since the gas located in the region of the discs interacts first with the wind, then both the MF and the gas are displaced farther form the galactic midplane whereas on the opposite portion of the discs ($x > 0$), the gas and the MF are compressed instead. For A90, the synchrotron emission is symmetric with respect to the $x = 0$ axis, as it was mentioned in §3.1, the MF has a water fountain appearance, hence there is some emission on the sides of the galactic midplane (in the reference frame of the galaxy is above and below the midplane). Here we shown the distribution of the total synchrotron emission at $t = 570$ given that it resembles the morphology observed in some Virgo Cluster galaxies, e.g. A0 and A20 with NGC 4522 (see fig. 3, 4 and 7 from Vollmer et al. 2004) or NGC 4330 (see fig. 4 from Vollmer et al. 2013) given that is truncated with the gaseous disc and spans on the opposite direction, and models A70 and A90 with NGC 4396, NGC 4402, and NGC 4654 (fig. 3, 4 and 8 from Vollmer et al. 2010).

4.1 Polarization

To determine the direction of the synchrotron polarization vectors, the emissivity parallel to the MF component in the plane of the sky $B_\perp$ is calculated

$$\varepsilon_\parallel = \varepsilon_{tot} \times \frac{(1+\Pi)}{2}\,, \tag{7}$$

where ε_{tot} is the total emissivity from eq. 6 and $\Pi = (p+1)/(p+7/3)$ is the degree of polarization of the emissivity. First, the emissivity over the y-axis is integrated in order to obtain the polarization vectors on the xz-plane. The parallel intensity over the y-axis is given by

$$I_{\parallel,x}(y+dy) = I_\parallel(y)\cos(\alpha) + \varepsilon(y)\cos(\alpha)\,dy = I_\parallel(y+dy)\cos(\beta) \tag{8}$$

$$I_{\parallel,z}(y+dy) = I_\parallel(y)\sin(\alpha) + \varepsilon(y)\sin(\alpha)\,dy = I_\parallel(y+dy)\sin(\beta)\,, \tag{9}$$

where α is the direction of $B_\perp$ measured in the x-axis and β is the direction of the inferred B-field,

$$\beta = \arctan\left(\frac{\int \varepsilon_\parallel \sin(\alpha)\,dy}{\int \varepsilon_\parallel \cos(\alpha)\,dy}\right)\,. \tag{10}$$

For the polarization vectors on the disc surface, that is, the xy-plane, $\varepsilon_\parallel$ was integrated along the z-axis.

Fig. 11 shows the B-vectors overlaid on maps of the

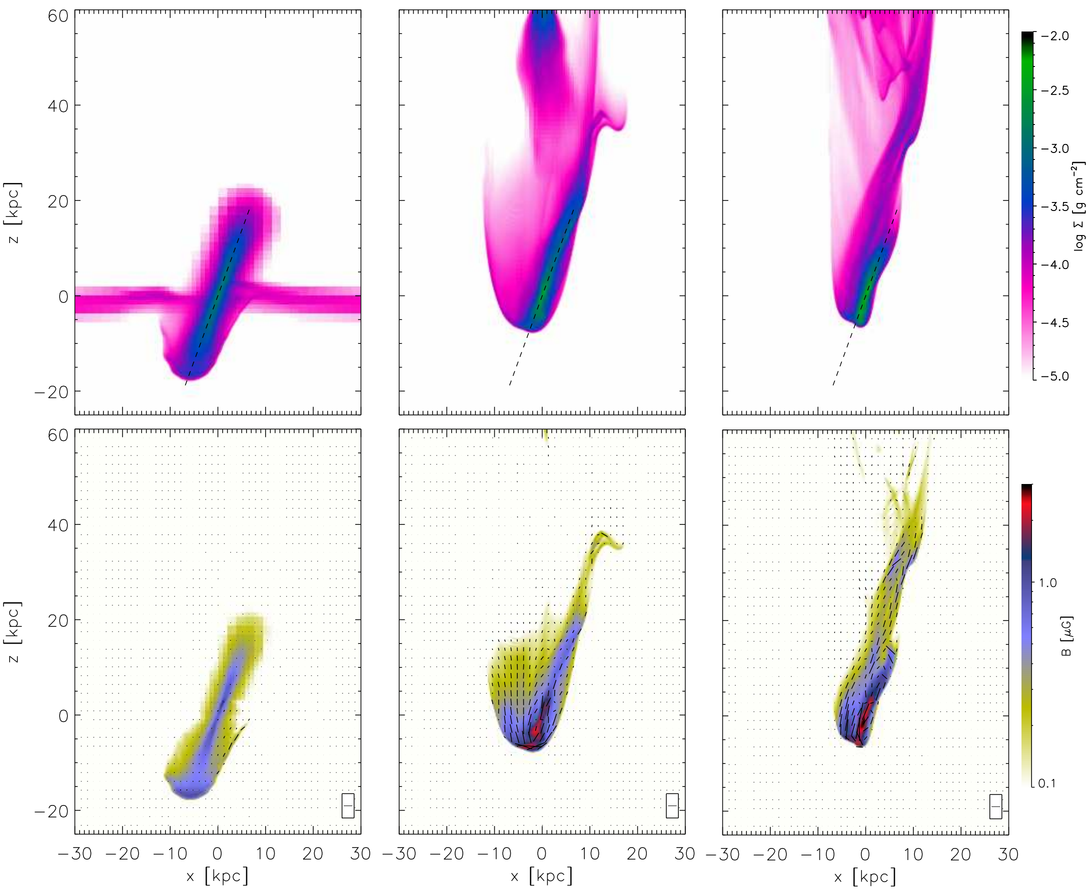

Figure 5. Same as fig. 2 for the A70 simulation.

surface density for the five runs at $t = 890\,\mathrm{Myr}$. The B lines have more random orientations in the tails of models A0, A20 and A45 (top panels) but still they tend to be aligned with the gas filaments and parallel to the surface of the remnant disc. Models A70 and A90 (bottom panels) have evolved more pasively since they show the same distribution during the simulation: on the downstream side the B lines run parallel along the elongated disc and tail while in the leading side they have a water fountain or concave shape. The distribution of the field for A70 and A90 is due to the way the discs are eroded, since the wind removes the gas above and below the galactic midplane, then the lines open on the leading side and wrap around the disc on the downstream side following the wind motion (see discussion in §3.1).

The synchrotron emission and the B-vectors were obtained from other LOS in the models, e.g. along the z-axis for A0 and A20, the x-axis for A70 and A90 and through both LOS for A45. The different directions for the LOS were chosen to be able to observe the entire disc surfaces. Fig. 12 (top panels) shows the synchrotron emission of models A0, A20 and A45 when integrating the emissivity along the z-axis, where it can be seen from the contours that the synchrotron is approximately symmetric at $|x| \lesssim 10\,\mathrm{kpc}$ which is the emission from the remnant disc while at larger radii ($|x| > 10\,\mathrm{kpc}$) is the projected distribution of gas and synchrotron from the filaments. In fig. 13 (top panels) the synchrotron emission for model A45, A70 and A90 is sharp on the leading side of the wind-disc interaction and extended over the opposite side along with the wind motion. There is also emission in filaments of the tails that resemble an unwound spiral structure.

The B-vectors for face-on views of the models A0, A20 and A45 are shown in the fig. 12 (bottom panels). They have a toroidal distribution with slight deviations between $r = 15-20\,\mathrm{kpc}$, at the filaments location, which means that the MFs remains circular in nearly face-on interactions but is perturbed in the vertical direction by the wind when its displaced with the gas. In models A70 and A90 (bottom panels in fig. 13), although the lines are toroidal in the disc, with $r \lesssim 10\,\mathrm{kpc}$ and surface density $\Sigma \gtrsim 10^{-3.5}\,\mathrm{g\,cm^{-2}}$, they tend to elongate along the z-axis, similar to ellipses with its major axis parallel to the wind motion. Also, in the two nearly edge-on models a spiral structure appears that spreads outside the disc to the downstream side (in the $+z$ direction), where the B-field also lines up vertically. Given that model A45 has an intermediate inclination, it shares properties with both low and high inclined discs. Also shown in fig. 13, the B-field configuration in model A45 is similar to A70 and A90, although the field lines are less extended along the z-axis in the disc region ($r < 10\,\mathrm{kpc}$), they are aligned with spiral-like structure unfolding to the tails.

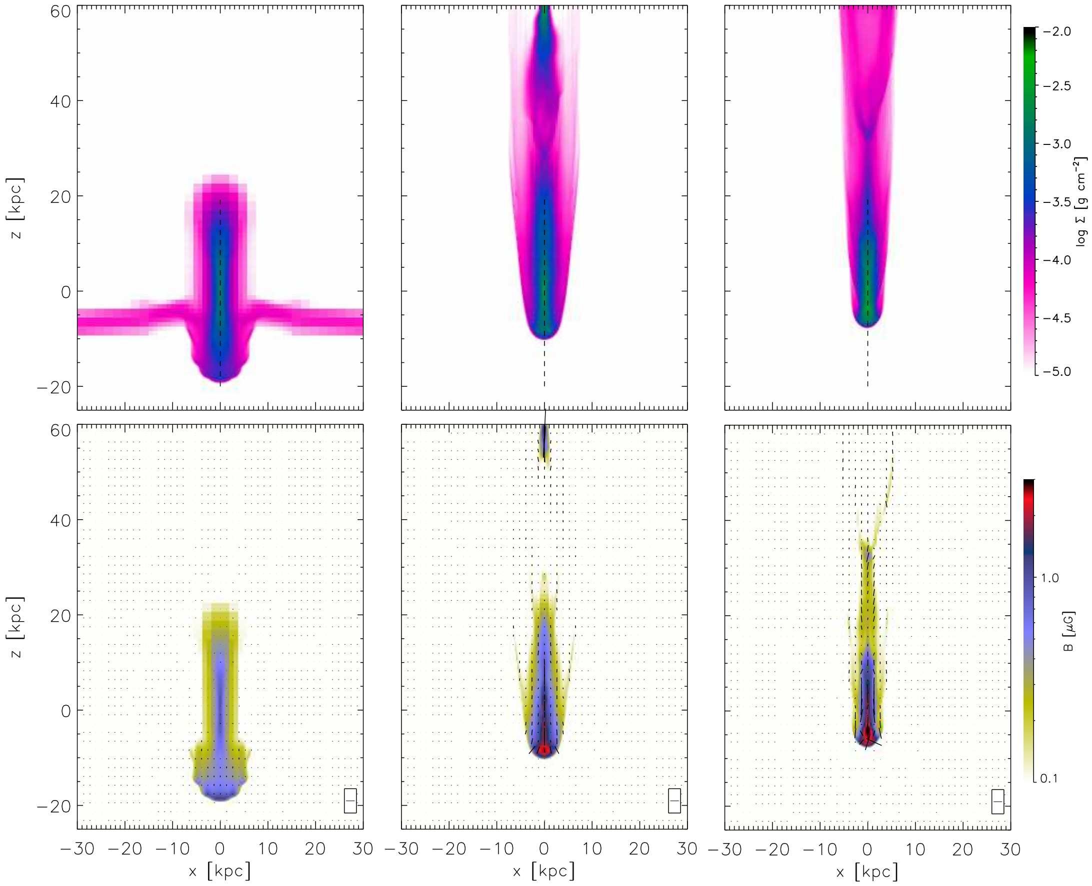

Figure 6. Same as fig. 2 for the A90 simulation.

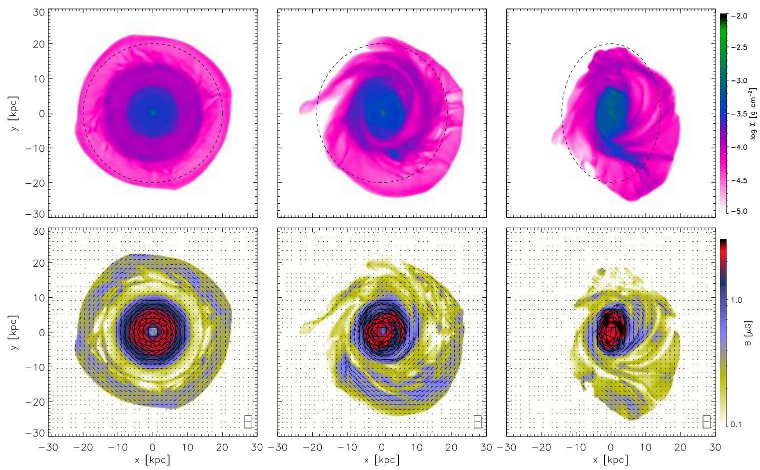

Figure 7. Gas surface density (*top row*) and magnetic field strength (*bottom row*) for models A0 (*left column*), A20 (*middle column*) and A45 (*right column*) at $t = 890\,$Myr in the xy-plane. The dashed lines in the top panels represents the initial size of the disc: $r = 20\,$kpc. The box in the bottom panels shows an MF line with a strength of $0.5\,\mu G$.

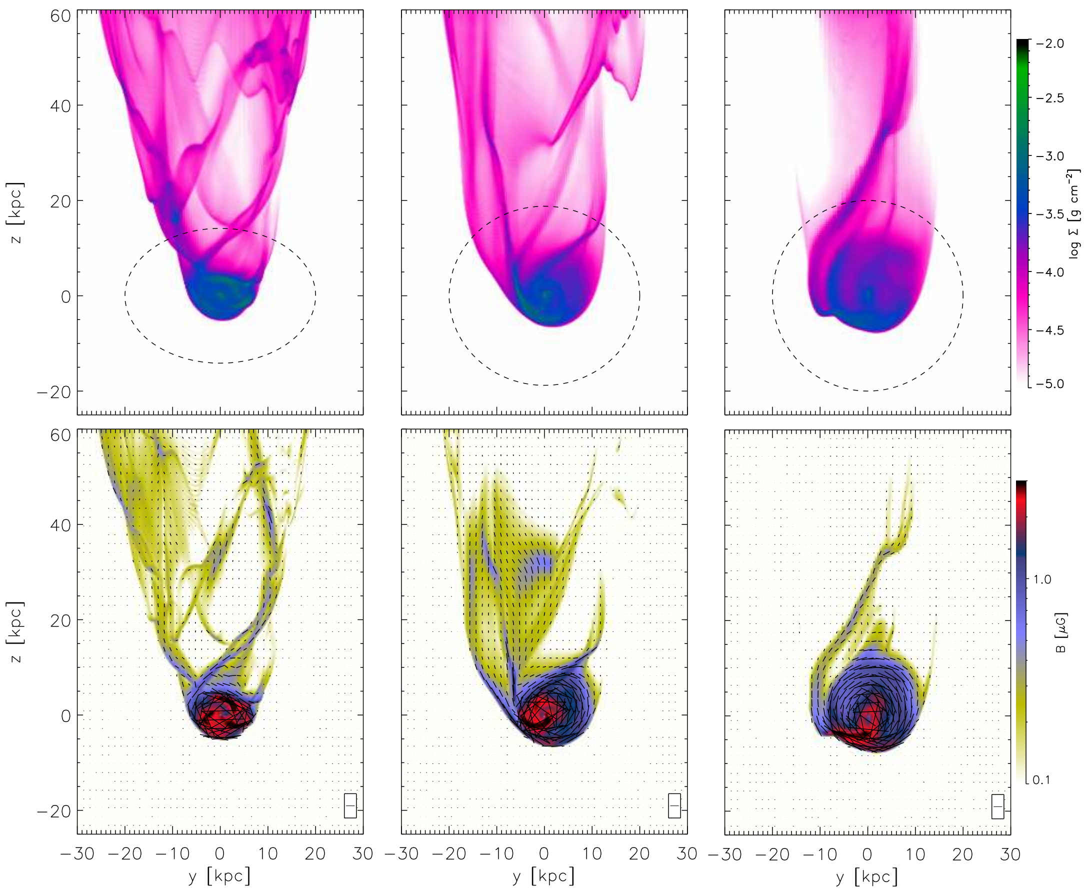

Figure 8. Same as fig. 7, for models A45 (*left column*), A70 (*middle column*) and A90 (*right column*).

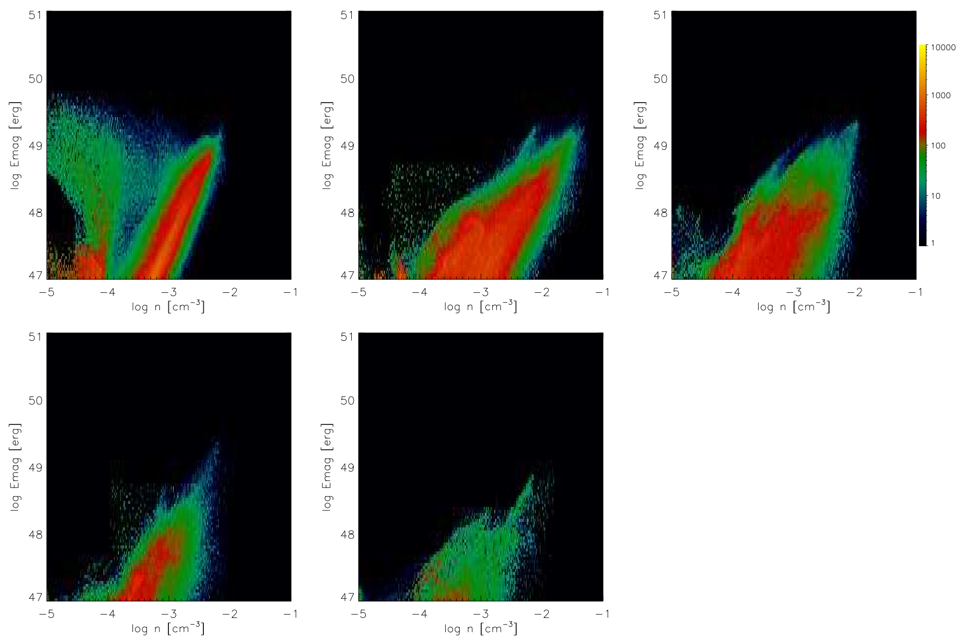

Figure 9. Histograms of magnetic energy and density at $t = 890\,\mathrm{Myr}$ for the five runs: disc tilted at 0^{O} (*top left*), 20^{O} (*top centre*), 45^{O} (*top right*), 70^{O} (*bottom left*) and 90^{O} (*bottom centre*), respectively.

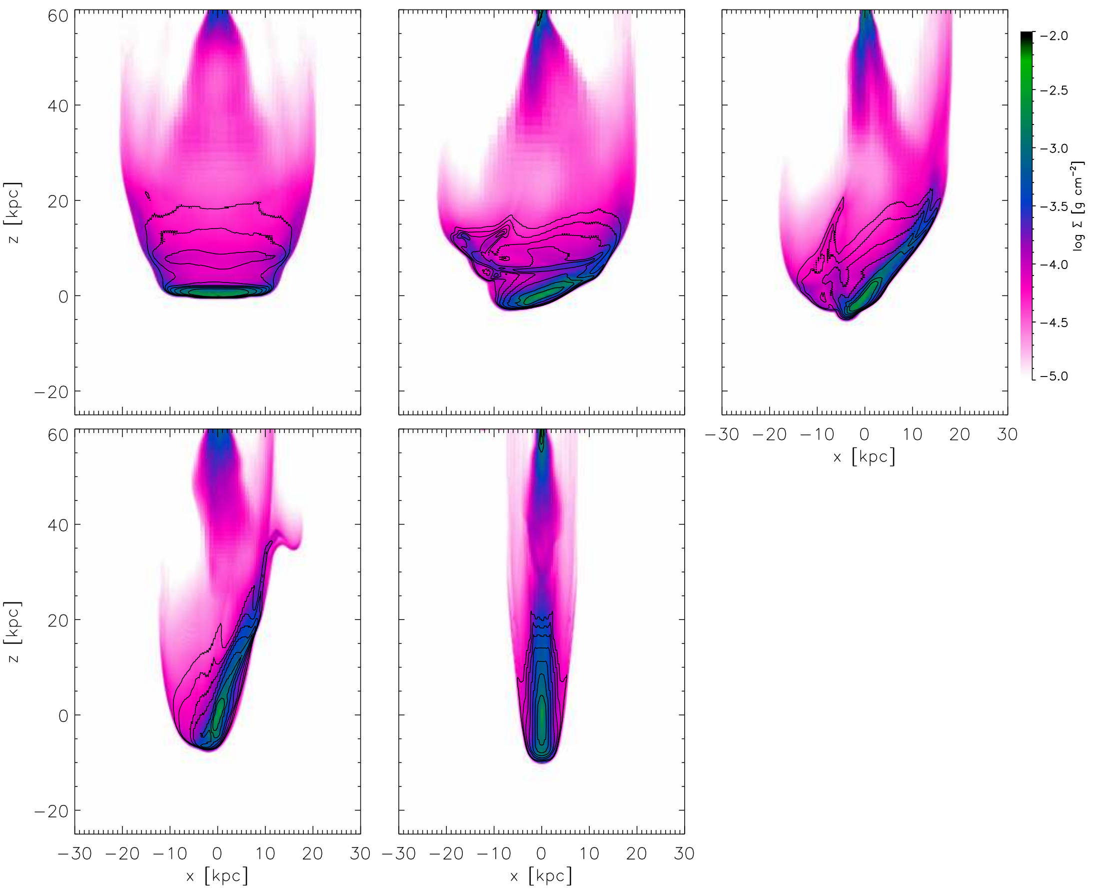

Figure 10. Total synchrotron emission distribution on a gas surface density map at t = 570 Myr for the four models: disc tilted at 0 (*top left*), 20 (*top centre*), 45^{o} (*top right*), 70 (*bottom left*) and 90^{o} (*bottom right*), respectively. The synchrotron emission is displayed in contours normalized to its maximum values and with levels $-2, -1.75, -1.5 - 0.75$ and -0.5 in log-scale. The gas surface density projected along the y-axis.

5 CONCLUSIONS

In this study, we presented MHD simulations of five tilted galaxies undergoing RPS in order to analyze the effects of the disc inclination in the gas removal. The inclination angle of the discs with respect to the $z = 0$ plane: 0, 20, 45, 70 and 90^{o}, which are denominated A0, A20, A45, A70 and A90, respectively.

The morphologies and properties observed in the tails for this simulations vary depending on the initial disc inclination. Once the ICM-wind starts to interact with the galaxies, it is observed that in models with (nearly) face-on geometry with respect to the wind motion, models A0 and A20, the gas is removed in ring-like structures and, since the MF and the gas are bound, the MF is also dragged by the wind. When the wind starts to remove gas from the disc, the rings of gas run parallel to the galactic plane up to 10−20 kpc above the disc at $t \gtrsim 500$ Myr with $B \approx 0.4 - 0.7\,\mu G$. When the gas is displaced farther from the galactic plane, the rings get distorted along the direction of the wind giving a filamentary structure to the tails, where also the MF is aligned with the filaments similarly to the results from Ruszkowski et al. (2014). Since these filaments are the densest structures in the tails, here the MF reaches its highest strength outside the discs, from $B \approx 0.3 - 0.4\,\mu G$ to $0.7\,\mu G$. In this interaction, the MF preserves its initial toroidal configuration during most of the time of the simulations with slight deviations in the region where the filaments are. For the nearly edge-on models, the MF lines emerge outside of the galactic plane in a "water fountain" shape wraping around the disc in the downstream side (at high z). Also, the MF lines have a structure similar to ellipses in the disc, that is, the MF is compressed in the wind-disc interaction zone and on the opposite side the MF is elongated and stretched when pushed by the wind. The tails in these models are not so prominent nor do they magnetize so much the surroundings, reaching values of $B \lesssim 0.2–0.3\,\mu G$, this means that the models with a low initial inclination contribute more to the magnetization of the ICM than models with a high inclined disc. Edge-on models also develop a spiral structure as a result of the combination of the ram pressure and the gas rotation, i.e. when the wind shocks with the disc where the gas sense of rotation has the same direction as the ram pressure, then the gas is stripped slightly easier and displaced farther of the galaxy; while in the side of the disc whose rotation opposes to the motion of the wind, the rotation itself prevents the gas of being swept and instead more material accumulates in that

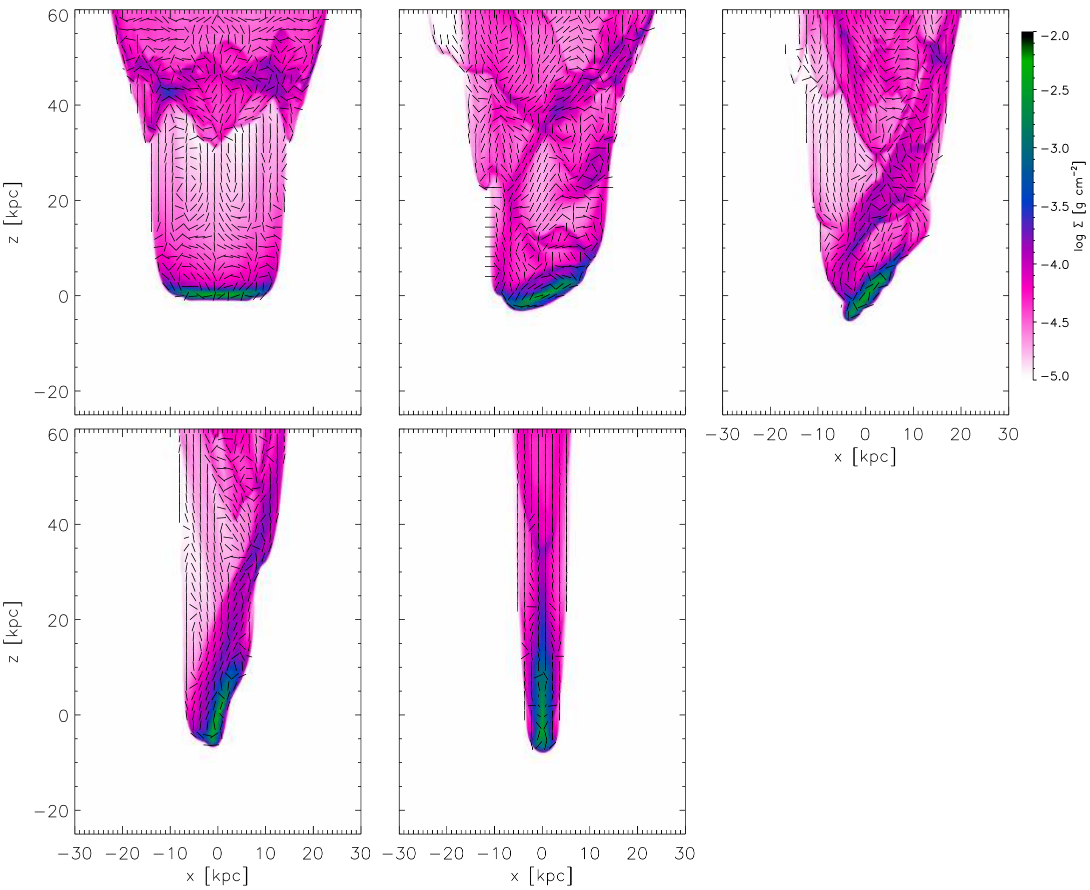

Figure 11. B-vectors inferred from the polarization of the synchrotron emission on a gas surface density map at $t = 890$ Myr for the five runs: A0 (*top left*), A20 (*top middle*), A45 (*top right*), A70 (*bottom left*) and A90 (*bottom right*), respectively. The gas surface density is projected along the y-axis.

part of the galaxy, generating a shape similar to spiral arms that also spreads downstream pushed by the wind, similar to the results of Tosa (1994) where a single-arm appears in an edge-on ram pressure stripped galaxy. The model A45, with an intermediate inclination, is a combination of models with low and high inclination: at $t \sim 500 - 600$ Myr evolves similarly to models A0 and A20, that is, the magnetized gas is removed in rings first, then at $t > 800$ Myr the tail of gas also develops filaments along the z-direction although it becomes narrower like models A70 and A90, also with $B \sim 0.3\,\mu G$, additionally, A45 presents a spiral-like morphology in the remnant discs which is observed also in the (nearly) edge-on cases.

Additionally, the MF strenght, at the end of the simulations ($t = 900$ Myr), reaches a maximum value of $B \sim 2 - 3\,\mu G$ which is a factor of ~ 3 higher than the initial one. However, in the models with low inclination, the increase is more homogeneous throughout the remnant disc, i.e. at all radii, whereas in the cases with inclinations $\geq 45^{\mathrm{o}}$ this occurs in the spiral-like structure. Observations of late-type spiral galaxies in clusters showed that they have a radio continuum emission enhanced by a factor up to ~ 5 compared to isolated spirals (Gavazzi & Jaffe 1986; Gavazzi & Boselli 1999) and this could be either by an increase in the star formation activity, producing more cosmic rays from supernovae, or an enhancement of the MF, or a combination of both.

We also obtained synchrotron emission maps and the B-vectors inferred from the polarization. The synchrotron emission presents an asymmetric distribution that is truncated in the disc and spreads out on the downstream side, following the gas. The maps of the emission from these simulations obtained at $t = 570$ Myr resemble the shape of the synchrotron tails of some Virgo galaxies, e.g. NGC 4522 (Vollmer et al. 2004), NGC 4330 (Vollmer et al. 2013), NGC 4396, NGC 4402, and NGC 4654 (Vollmer et al. 2010), despite the restrictions of the models presented in this work. The B-vectors trace very accurately the MF of the simulations: they line up with the filaments of gas observed in face-on interactions and follow the compressed gas in the upstream side of the disc and are more elongated in the downstream side of the edge-on models. Since the MFs lines in these simulations change depending on the disc inclination, the distribution of the synchrotron and the B-vectors inferred from the polarization can have also information of the wind direction in galaxies travelling through a cluster. Additionally, the gas is easy to perturb in tidal interactions or RPS, so it will still be reflected on the MFs through com-

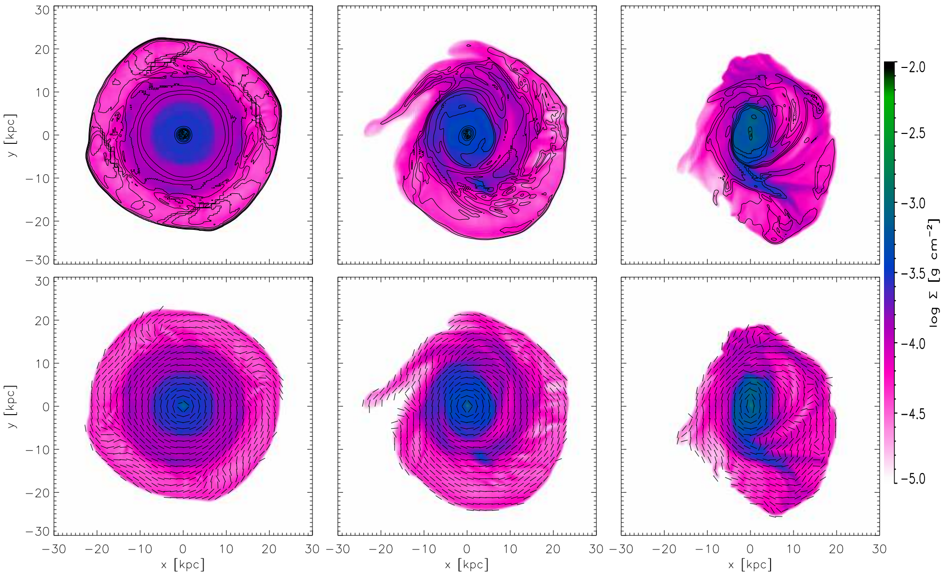

Figure 12. Total synchrotron emission distribution (*top row*) and the *B*-vectors inferred from the polarization of the synchrotron emission (*bottom row*) on a gas surface density map at $t = 890\,$Myr for A0 (*left column*), A20 (*middle column*) and A45 (*right column*). The synchrotron emission is displayed in contours normalized to its maximum values and with levels −2, −1.75, −1.5, −0.75 and −0.5 in log-scale. The gas surface density projected along the z-axis.

pression or shear motions, leaving an imprint in the synchrotron and polarization emission.

ACKNOWLEDGEMENTS

We thank Alice Pasetto and Bianca Poggianti for useful comments and discussions. We acknowledge financial support from UNAM-DGAPA PAPIIT grant IN100916 and CONACyT (México).

REFERENCES

Adebahr B., Krause M., Klein U., Weżgowiec M., Bomans D. J., Dettmar R.-J., 2013, A&A, 555, A23
Beck R., 2005a, in Chyzy K. T., Otmianowska-Mazur K., Soida M., Dettmar R.-J., eds, The Magnetized Plasma in Galaxy Evolution. pp 193–200
Beck R., 2005b, in Wielebinski R., Beck R., eds, Lecture Notes in Physics, Berlin Springer Verlag Vol. 664, Cosmic Magnetic Fields. p. 41, doi:10.1007/11369875_3
Beck R., Wielebinski R., 2013, Magnetic Fields in Galaxies. p. 641, doi:10.1007/978-94-007-5612-0_13
Beck R., Fletcher A., Shukurov A., Snodin A., Sokoloff D. D., Ehle M., Moss D., Shoutenkov V., 2005, A&A, 444, 739
Bonafede A., Feretti L., Murgia M., Govoni F., Giovannini G., Dallacasa D., Dolag K., Taylor G. B., 2010, A&A, 513, A30
Bonafede A., Govoni F., Feretti L., Murgia M., Giovannini G., Brüggen M., 2011, A&A, 530, A24
Bonafede A., Vazza F., Brüggen M., Murgia M., Govoni F., Feretti L., Giovannini G., Ogrean G., 2013, MNRAS, 433, 3208
Carilli C. L., Taylor G. B., 2002, ARA&A, 40, 319
Chyży K. T., Beck R., 2004, A&A, 417, 541
Chyży K. T., Soida M., Bomans D. J., Vollmer B., Balkowski C., Beck R., Urbanik M., 2006, A&A, 447, 465
Chyży K. T., Ehle M., Beck R., 2007, A&A, 474, 415
Clarke T. E., Kronberg P. P., Böhringer H., 2001, ApJ, 547, L111
Fendt C., Beck R., Neininger N., 1998, A&A, 335, 123
Feretti L., Dallacasa D., Govoni F., Giovannini G., Taylor G. B., Klein U., 1999, A&A, 344, 472
Ferrière K., 1998, ApJ, 497, 759
Fletcher A., 2010, in Kothes R., Landecker T. L., Willis A. G., eds, Astronomical Society of the Pacific Conference Series Vol. 438, The Dynamic Interstellar Medium: A Celebration of the Canadian Galactic Plane Survey. p. 197 (`arXiv:1104.2427`)
Fletcher A., Beck R., Shukurov A., Berkhuijsen E. M., Horellou C., 2011, MNRAS, 412, 2396
Fosalba P., Lazarian A., Prunet S., Tauber J. A., 2002, ApJ, 564, 762
Frick P., Stepanov R., Beck R., Sokoloff D., Shukurov A., Ehle M., Lundgren A., 2016, A&A, 585, A21
Gavazzi G., Boselli A., 1999, A&A, 343, 93
Gavazzi G., Jaffe W., 1986, ApJ, 310, 53
Gießübel R., 2012, PhD thesis, Univ. Cologne, `https://kups.ub.uni-koeln.de/5004/`
Giovannini G., Feretti L., Venturi T., Kim K.-T., Kronberg P. P., 1993, ApJ, 406, 399
Gómez G. C., Cox D. P., 2002, ApJ, 580, 235
Govoni F., Feretti L., 2004, International Journal of Modern Physics D, 13, 1549
Govoni F., et al., 2010, A&A, 522, A105
Greaves J. S., Holland W. S., Jenness T., Hawarden T. G., 2000, Nature, 404, 732
Han J. L., Ferriere K., Manchester R. N., 2004, ApJ, 610, 820
Han J. L., Manchester R. N., Lyne A. G., Qiao G. J., van Straten W., 2006, ApJ, 642, 868
Jones T. J., 2000, AJ, 120, 2920
Kim K.-T., Kronberg P. P., Dewdney P. E., Landecker T. L., 1990, ApJ, 355, 29
Kim K.-T., Tribble P. C., Kronberg P. P., 1991, ApJ, 379, 80
Klein U., Weiland H., Brinks E., 1991, A&A, 246, 323
Kronberg P. P., 2005, in Wielebinski R., Beck R., eds, Lecture

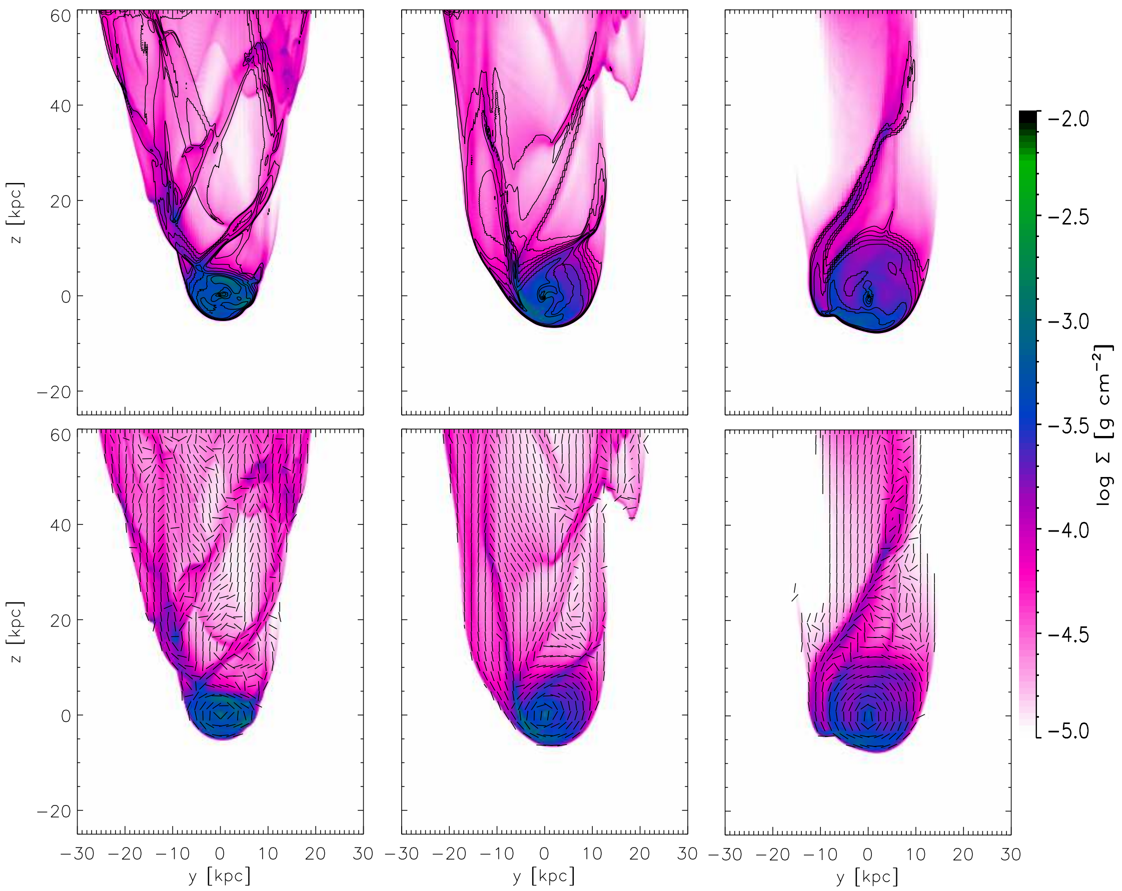

Figure 13. Total synchrotron emission distribution (*top row*) and the *B*-vectors inferred from the polarization of the synchrotron emission (*bottom row*) on a gas surface density map at $t = 890$ Myr for A45 (*left column*), A70 (*middle column*) and A90 (*right column*). The synchrotron emission is displayed in contours normalized to its maximum values and with levels −2, −1.75, −1.5, −0.75 and −0.5 in log-scale. The gas surface density projected along the x-axis.

Notes in Physics, Berlin Springer Verlag Vol. 664, Cosmic Magnetic Fields. p. 9, doi:10.1007/11369875_2
Miley G., 1980, ARA&A, 18, 165
Murgia M., Govoni F., Feretti L., Giovannini G., Dallacasa D., Fanti R., Taylor G. B., Dolag K., 2004, A&A, 424, 429
Murphy E. J., Kenney J. D. P., Helou G., Chung A., Howell J. H., 2009, ApJ, 694, 1435
Niklas S., 1995, PhD thesis, Univ. Bonn
Ohno H., Shibata S., 1993, MNRAS, 262, 953
Orlando E., Strong A., 2013, MNRAS, 436, 2127
Otmianowska-Mazur K., Vollmer B., 2003, A&A, 402, 879
Pfrommer C., Jonathan Dursi L., 2010, Nature Physics, 6, 520
Ramos-Martínez M., Gómez G. C., Pé rez-Villegas Á., 2018, MNRAS, 476, 3781
Rand R. J., Kulkarni S. R., 1989, ApJ, 343, 760
Rudnick L., Blundell K. M., 2003, ApJ, 588, 143
Ruszkowski M., Brüggen M., Lee D., Shin M.-S., 2014, ApJ, 784, 75
Ryu D., Schleicher D. R. G., Treumann R. A., Tsagas C. G., Widrow L. M., 2012, Space Sci. Rev., 166, 1
Scarrott S. M., Ward-Thompson D., Warren-Smith R. F., 1987, MNRAS, 224, 299
Soida M., Otmianowska-Mazur K., Chyży K., Vollmer B., 2006, A&A, 458, 727
Tabatabaei F. S., Krause M., Fletcher A., Beck R., 2008, A&A, 490, 1005
Taylor G. B., Perley R. A., 1993, ApJ, 416, 554
Taylor G. B., Barton E. J., Ge J., 1994, AJ, 107, 1942
Taylor G. B., Govoni F., Allen S. W., Fabian A. C., 2001, MNRAS, 326, 2
Tonnesen S., Stone J., 2014, ApJ, 795, 148
Tosa M., 1994, ApJ, 426, 81
Vacca V., Murgia M., Govoni F., Feretti L., Giovannini G., Perley R. A., Taylor G. B., 2012, A&A, 540, A38
Vallée J. P., 1997, Fundamentals Cosmic Phys., 19, 1
Vallée J. P., MacLeod M. J., Broten N. W., 1986, A&A, 156, 386
Vallée J. P., MacLeod J. M., Broten N. W., 1987, Astrophys. Lett., 25, 181
Vijayaraghavan R., Sarazin C., 2017, ApJ, 848, 63
Vollmer B., Beck R., Kenney J. D. P., van Gorkom J. H., 2004, AJ, 127, 3375
Vollmer B., Soida M., Otmianowska-Mazur K., Kenney J. D. P., van Gorkom J. H., Beck R., 2006, A&A, 453, 883
Vollmer B., Soida M., Beck R., Urbanik M., Chyży K. T., Otmianowska-Mazur K., Kenney J. D. P., van Gorkom J. H., 2007, A&A, 464, L37
Vollmer B., Soida M., Chung A., Beck R., Urbanik M., Chyży K. T., Otmianowska-Mazur K., van Gorkom J. H., 2010, A&A, 512, A36
Vollmer B., Soida M., Beck R., Chung A., Urbanik M., Chyży K. T., Otmianowska-Mazur K., Kenney J. D. P., 2013, A&A, 553, A116

This paper has been typeset from a TEX/LATEX file prepared by the author.